Rare earth co-doped ZnO photocatalysts: Solution combustion synthesis and environmental applications

I. Ahmad, Muahmmad Shoaib Akhtar, Ejaz Ahmed, Mukhtar Ahmad, Valérie Keller, Waheed Qamar Khan, N.R. Khalid

Separation and Purification Technology 237 (2020) 116328

Contents lists available at ScienceDirect

Separation and Purification Technology

journal homepage: www.elsevier.com/locate/seppur

Rare earth co-doped ZnO photocatalysts: Solution combustion synthesis and environmental applications

I. Ahmad[a,*], Muahmmad Shoaib Akhtar[b], Ejaz Ahmed[a], Mukhtar Ahmad[a], Valérie Keller[c], Waheed Qamar Khan[d], N.R. Khalid[e]

[a] Department of Physics, Bahauddin Zakariya University, Multan 60800, Pakistan
[b] School of Computer and Communication, Lanzhou University of Technology, Lanzhou 10731, China
[c] Institut de Chimie et Procédés pour l'Energie, l'Environnement et la Santé (ICPEES), CNRS UMR 7515, University of Strasbourg, 25 rue Becquerel, 67087 Strasbourg Cedex, France
[d] Institute of Advanced Materials, Bahauddin Zakariya University, Multan 6800, Pakistan
[e] Department of Physics, University of Gujrat, Pakistan

ARTICLE INFO

Keywords:
Combustion route
Photocurrent
Photocatalyst
MB degradation
H_2 generation

ABSTRACT

A novel europium (Eu) and terbium (Tb) co-doped ZnO nanoparticles had been synthesized by a facile, cost efficient and rapid combustion method. The physical and chemical properties of the as-synthesized nanoparticles were determined by XRD, SEM, EDS, BET, FTIR, XPS, UV–vis DRS, PL, EIS and photocurrent density. XRD patterns confirm that Eu and Tb ions are stably inserted into the framework of ZnO, and the crystallite size decreases to 21 nm compared to that of pure ZnO (32 nm) as the amount of co-dopants increases to optimal value (3 mol% of each). With the insertion of Eu and Tb ions into ZnO, the recombination rate of photo generated charge carriers is found to be low. It is observed that doped Eu and Tb ions can enter the lattice structure of ZnO with a suitable doping concentration, and the obtained doped ZnO have ordered hexagonal wurtzite structures and nearly spherical morphology with high specific surface area and high porosity. Meanwhile, the introduction of Eu and Tb ions can effectively extend the spectral response from UV to visible region for the catalysts, thus reducing the band gap from 3.25 to 2.91 eV. Further analysis by means of XPS measurement showed that the existence of mixture of Eu^{2+}/Eu^{3+} and Tb^{3+}/Tb^{4+} oxidation states and high content of the surface chemisorbed oxygen species also contributed to the high photocatalytic activity. It was found that Eu and Tb co-doped ZnO shows highly efficient and stable visible light activity and provides a 100% MB degradation within 15 min, while the degradation time for Eu doped ZnO and Tb doped ZnO is reduced gradually to 50 and 42 min, respectively to obtain the 100% MB degradation. It was also found that the photocatalytic hydrogen evolution activity over Eu and Tb co-doped ZnO can be significantly increased to 533.8 and 792 μmol with 0.2 wt% catalyst dose and initial solution pH 9, respectively under similar conditions with good stability. Moreover, simultaneous introduction of Eu and Tb effectively promoted the yield of CH_4 to 4.59 μmol, which was 3.4 fold higher in comparison to pure ZnO. Thus the present approach could provide a versatile strategy for the synthesis of novel and efficient visible light activated photocatalysts.

1. Introduction

Recent reports suggest that water pollution from various industries such as textile, leather, paper and plastic has become a severe world-wide problem, resulting in harmful influence on the environment. Among them, dyes play an important role towards environment contamination. The traditional pathways such as adsorption, biodegradation, chlorination and ozonation still undesirably give rise to numerous drawbacks, such as non-recyclability, low adsorption capacity, and complex operations for recycling.

Photocatalytic degradation is considered as a promising and preferred methodology for waste water treatment due to its biological and chemical inertness, strong capacity, cost effectiveness, and long term stability against photo and chemical corrosion. Today, the world is also continuously succeeding towards the expected threat of energy crisis because of the rapid elimination of fossil fuels due to its non-renewable fact [1]. Hydrogen is a clean and green fuel. The conversion and store solar energy in the form of hydrogen by photocatalytic water splitting

* Corresponding author at: Department of Physics, Bahauddin Zakariya University, Multan 60800, Pakistan.
E-mail address: irshadmahar55@yahoo.com (I. Ahmad).

https://doi.org/10.1016/j.seppur.2019.116328
Received 29 August 2019; Received in revised form 16 November 2019; Accepted 17 November 2019
Available online 19 November 2019

holds great promise to meet the future energy and environment requirement [2]. Solar fuel production from H_2O and CO_2 is an ideal counter measure for the energy and environmental concerns the world is facing today. The environmental changes can be controlled by conversion of CO_2 in to CH_4, H_2O and H_2 fuels [3]. Photocatalytic activity is considered as a promising and preferred methodology for waste water treatment, hydrogen generation and reduction of CO_2 due to only light source requirement. Among semiconductor photocatalysts, TiO_2 (3.20 eV), ZnO (3.37 eV) and WO_3 (2.50 eV) have demonstrated most encouraging activities for photocatalytic applications [4–6].

ZnO is inexpensive and wide band gap semiconductor that corresponds to wavelength of ~375 nm and applied in the field of energy and environmental remediation processes because of its high photo reactivity, great photostability, exceptional stability, non-toxicity and low cost, but photocorrosion, backward reaction, poor stability and visible light absorption inability are the documented impediments of ZnO [7]. Numerous modifications have been attempted to overcome these problems such as doping with metals and non-metals ions [8,9], coupling with other semiconductors [10] and etc. In order to utilize light illumination effectively, doping of photocatalysts with RE metals not only improve the photocatalytic efficiency but also increase the electron hole separation [11]. The rare earth metals have the incomplete 4f orbital configuration beneficial to trap the electron in order to reduce the recombination of charge carriers and enhance the catalytic activity ascribed to high surface area and excellent electrons trap ability due to mixed chemical (+2, +3, +4) sites. Huo et al reported sol gel synthesized yttrium and aluminum co-doped ZnO photocatalyst for hydrogen evolution. The enhanced hydrogen evolution was assigned to increased light absorption and decreased band gap [12]. Anorkon et al reported sono-chemical synthesized Eu doped ZnO photocatalyst towards waste treatment [13].

In present work, Eu and Tb co-doped ZnO nanoparticles were synthesized via combustion method for photocatalytic MB degradation, H_2 generation and CO_2 reduction. The characteristic of variable valence resulting in distinct Eu^{3+}/Eu^{2+} and Tb^{4+}/Tb^{3+} chemical states and relative stable configuration of Eu and Tb due to half filled in the 4f orbital that confine 7f-electrons stimulated us for the selectivity of Eu and Tb. To the best of our knowledge, there has been no report for Eu and Tb co-doped ZnO for photocatalytic application. The impact of Eu and Tb doping on the structural, morphological, optical and photocatalytic properties for MB degradation, hydrogen generation and CO_2 reduction under visible light illumination was studied in detail.

2. Experimental

2.1. Synthesis and characterization

Auto-combustion method was used to design pure ZnO and Eu and Tb doped ZnO nanoparticles $Eu_xTb_xZn_{1-2x}O$ (x = 0, 1.5 wt% and 3 wt %) using zinc nitrate ($Zn(NO_3)_2{\cdot}6H_2O$), europium nitrate ($Eu(NO_3)_3{\cdot}9H_2O$) (99.9%), terbium nitrate ($Tb(NO_3)_3{\cdot}6H_2O$) (99.9%), and glycine ($C_2H_5NO_2$). All reagents were purchased from Merck Company and used without further purification. The balance between valencies of the oxidant and fuel is significant to calculate the stoichiometric composition of the mixture, which will consequently result in evolution of maximum energy for each reaction. The thermo-chemical concepts reveal that Zn, Eu, Tb, H and C contain +2, +3, +3, +1 and +2 valencies, respectively and acts as reducing element [11]. O element contains −2 valency acts as oxidizing agent, while zero valency corresponds to N element. Thus total valencies in ($Zn(NO_3)_2{\cdot}6H_2O$) add up to −10 and in ($Eu(NO_3)_3{\cdot}9H_2O$) and ($Tb(NO_3)_3{\cdot}6H_2O$) add up to −15 for each, should be equal to total valencies in the fuel which add up to +9. Thus, the requirement for stoichiometric composition to show the maximum energy for thermo-chemical reaction to synthesize $Eu_xTb_xZn_{1-2x}O$ is 5x + 10 = 6n or n = 1.67 mol of Glycine. Initially stoichiometric composition of all reagents was mixed in a glass beaker and placed in air without protection from nitrogen. Zinc nitrate absorb moisture due to its hygroscopic nature and turned into transparent slurry. Afterword, the heat treatment (~180 °C) was given to slurry on hot plate with constant magnetic stirring to make homogeneous solution for 2 h. When temperature of hot plate is enhanced to 350 °C, the color of the solution was varied from white to red, red to yellow, yellow to light brown, light brown to dark brown and finally turned into blackish gel with lengthening time and constant stirred process. Afterword, the solution began thickened and lathering, following ignition with characterized by quick enhance of temperature and evolution of large amount of non-toxic gases. The reactions were exothermic and lasted a few seconds, resulting in dry, loose and voluminous soft foam that changed in to nano-powder at the slightest touch. These nanopowders were further calcined at 700 °C to absorb any remained moisture and to develop fine nanoparticles as final product in white color. ZnO doped with 3 mol % of Eu and Tb was named as EZO and TZO, respectively. ZnO co-doped with 1.5 and 3 mol% of europium and terbium was labeled as ETZ1 and ETZ2, respectively. The following reactions occurred during combustion process

$$Zn(NO_3)_2{\cdot}6H_2O + Eu(NO_3)_3{\cdot}9H_2O + Tb(NO_3)_3{\cdot}6H_2O \rightarrow Eu_xTb_x ZnO_{1-2x} + H_2O\text{vapors} + CO_2 + N_2 \quad (1)$$

The ZnO and ETZ nanoparticles were characterized using XRD (Xpert PRO-MPD, Philips), SEM (FEI sirion 200), EDS (EX-250), XPS (AXIS-NOVA, CJ109) Krates, lnc), FTIR (Nicolet Avatar 360 FTIR), BET (Germini-2375, Shimadzu), UV–visible DRS (Cary 500 spectrometer), PL (Perkin Elmer) and photocurrent density (CompactStat, IVIUM STAT tech.).

2.2. Photocatalytic activity

The photocatalytic activity of ZnO and doped ZnO catalysts was evaluated by the degradation of 100 mg/L MB solution in a Pyrex reactor with an effective vessel volume of 500 mL. 300 W xenon light with refrigerating water circuit acted as a slide light source. An aliquot of 1 mL was withdrawn after certain time period of illumination and centrifuged to separate the nanoparticles. At the end, centrifugates were examined by recording the absorbance of MB.

Typically, photocatalysts (20 mg) was dispersed using a magnetic stirrer in 60 mL methanol aqueous solution for the photocatalytic hydrogen generation. Then suspension was purged with an argon flow for minimum 30 min to remove the residual air prior to illumination. Constant stirring was carried out to ensure the suspension status during photoreaction. The generation of hydrogen was confirmed by withdrawn of gas product at periodic interval by 0.5 mL syringe (Hamilton, USA) and analyzed through a gas chromatograph (GC-8A, MS-5A column, TCD, Shimadazu, Japan).

CO_2 reduction was carried out at atmospheric pressure and room temperature. In a typical experiment, 100 mg of the sample was put into the reactor and 10 mL of deionized water added. Before irradiation, the reactor was blown with nitrogen for 30 min to remove air, and to ensure that the reaction system was under anaerobic conditions. After light illumination for 1 h, 1 mL of evolved gas product was extracted from the reactor, which was then detected by a gas chromatograph (GC-8A, MS-5A column, TCD, Shimadazu, Japan). Products were calibrated with a standard CH_4 gas by using a gas chromatograph (GC-8A, MS-5A column, TCD, Shimadazu, Japan). The carrier gas used in the GC-2014C was high purity nitrogen.

3. Results and discussions

3.1. XRD analysis

Fig. 1 shows the XRD pattern of ZnO and ETZ materials. The diffraction peaks are in good agreement with the JCPDS No. 36-1451,

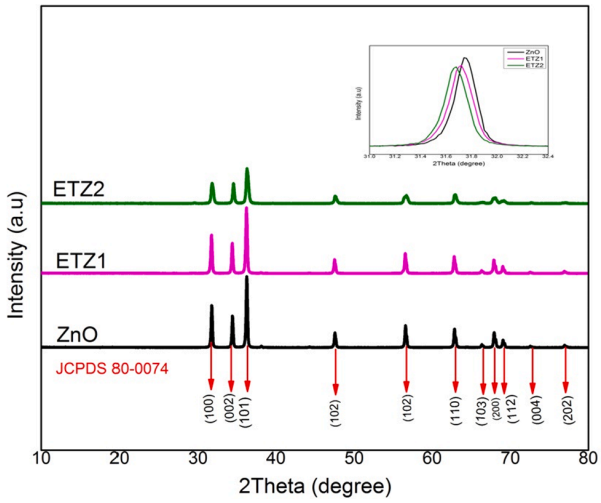

Fig. 1. XRD pattern of ZnO and ETZ photocatalysts.

Table 1
Crystallite size and lattice constants of pure ZnO, EZO, TZO, ETZ1 and ETZ2 nanoparticles.

Sample name		ZnO	EZO	TZO	ETZ1	ETZ2
Crystallite size (nm)		32	29	28	26	21
Lattice constants (nm)	a	0.324	0.325	0.325	0.327	0.328
	c	0.524	0.525	0.524	0.528	0.530

showing that the crystal structure of ETZ synthesized by the solution combustion method is the typical crystalline wurtzite hexagonal phase of ZnO. There were no other peaks corresponding to metallic europium and terbium, indicating that the as-synthesized samples are of single phase. The broad diffraction peaks also indicate that sample has deteriorated crystallinity. No peaks associated with other impurity phases were detected in the XRD pattern. The diffraction peaks of ETZ shifted towards lower angles than peaks of pure ZnO (JCPDS No. 76-0704). This could be attributed to the larger covalent radii difference of Eu^{3+} (95 pm) and Tb^{3+} (104 pm) than Zn^{2+} (74 pm) [14]. Thus, Eu and Tb substitution for Zn in ZnO will induce the expansion of the crystal lattice and lead to the lower angle shifts of the diffraction peaks. The diffraction peak (0 0 2) of crystal plane was selected to estimate the crystallite size of the sample by the Debye Scherrer equation and is given in Table1. The calculated values of lattice constants are also given in Table1.

3.2. SEM, BET surface area and EDS analysis

Fig. 2a and b shows the SEM images of the synthesized samples. Fig. 2a shows nearly spherical, homogeneous and randomly distributed nanoparticles. When Eu and Tb were added to starting material, the obtained ZnO still showed spherical like structure, but a porous structure agglomerated with very small particles size ranging from 13 to 21 nm (Fig. 2b), which is mainly assembled by nanoparticles. The agglomeration is made up of ZnO and nanoparticles of Eu and Tb are dispersed on the surface of ZnO. The large amount of the agglomeration in the nanoparticles should be beneficial to enlarge the contact area for enhanced reactant diffusivity, which is highly favorable for catalytic activity [15]. The specific surface area observed for ZnO found to be 38.12 $m^2\ g^{-1}$, which is very less in comparison to ETZ2 and that is 74.21 $m^2\ g^{-1}$. It is anticipated that observed increment in the surface area could be one of the factors responsible for the enhanced photocatalytic activity of the Eu and Tb co-doped ZnO nanoparticles. EDS mapping results are shown in Fig. S1. The presence of Zn, O, Eu and Tb

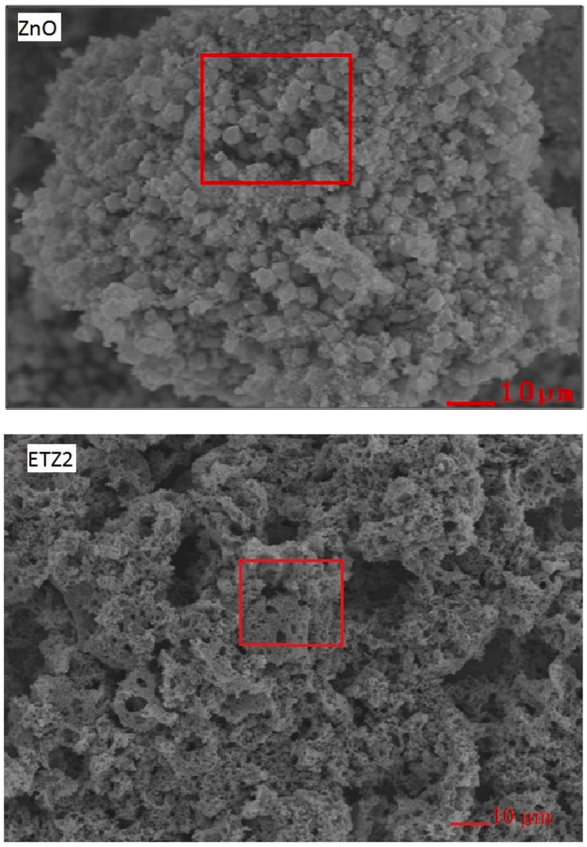

Fig. 2. SEM analysis of ZnO and ETZ2 photocatalysts.

elements in ETZ2 catalyst confirms the successful decoration of both the metals in ZnO. No traces of other impurity elements were observed in the spectra, implying that the synthesized samples are pure. The atomic percentage of elements in pure ZnO and ETZ2 is shown in Table S1. The atomic percentages clearly indicate oxygen vacancy in composition that will be consequently beneficial for the adsorption process which plays the role of residual centers; eventually promote the photocatalytic performance [16].

3.3. FTIR analysis

To evaluate the presence of all the functional groups in ZnO and doped ZnO nanoparticles, FTIR study was performed as shown in Fig. S2. The peaks at 3115 and 3442 cm^{-1} can be attributed to stretching of O–H vibrations group whose intensity was increased to some extent due to successful introduction of Eu^{3+} and Tb^{3+} ions, suggesting expansion of lattice. Photocatalytic performance strongly depends on number of O–H groups on photocatalyst surface due to oxidizing capability of O–H group to transform into reactive hydroxyl radicals (*OH) [17]. The peaks at 2850 cm^{-1} can be attributed to stretching of C–H group, while the peaks at 2322 and 1636 cm^{-1} are due to the presence of CO_2, bending vibrations of adsorbed water on the photocatalyst surface, respectively. In addition, a broad peak at 505 cm^{-1} is observed due to stretching vibration of tetrahedral Zn^{2+} and Eu^{3+} and Tb^{3+} ions (Zn–O and Eu–O, Tb–O mode) of ZnO, suggesting Eu and Tb are successfully doped into ZnO lattice [18].

3.4. UV–vis absorption spectra analysis

The absorption spectra of the photocatalysts are shown in Fig. 3. The optical absorption edge for pure ZnO appears at 381 nm because of

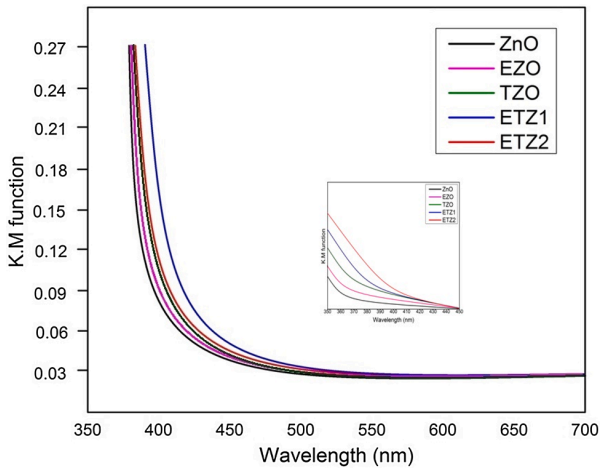

Fig. 3. UV–vis absorption spectra of ZnO and doped ZnO photocatalysts.

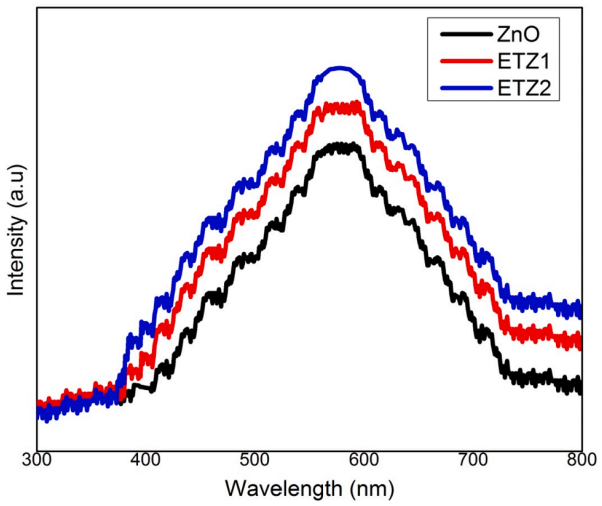

Fig. 4. PL analysis of ZnO and ETZ photocatalyst.

its wide optical band gap, which indicates that ZnO is only active under UV-light illumination. It is seen that doped ZnO materials possess longer wavelength absorption than pure ZnO. Photocatalyst EZO shows an optical response at 394 nm due to the effect of Eu substitution into the ZnO lattice, while TZO shows absorption response at 397 nm due to introduction of Tb into lattice of host ZnO. However, ETZ1 exhibit absorption in the visible region at 407 nm, which further shift to 427 nm for ETZ2 sample [19]. Thus, the co-existence of Eu and Tb in ZnO sites can shift the light absorption range of ZnO from the UV to the visible region, leading to improved catalytic activity under visible light illumination. The inset of Fig. 3 shows enhancement in the optical absorption towards longer wavelength with increase in dopants is caused by the increase of oxygen vacancies in the catalyst crystal structure which can inhibit the recombination of the charge carriers and enhances the photocatalytic activity of the catalyst. The optical band gaps of the materials were estimated using the 1240/wavelength (nm) relationship [20]. The calculated optical band gap energies of ZnO, EZO, TZO, ETZ1 and ETZ2 are 3.25, 3.15, 3.12, 3.04 and 2.91 eV, respectively. Thus, the lowest optical band gap is observed for the ETZ2 photocatalyst. Similar shifts in band gap have been reported by many researchers [19–21].

3.5. PL analysis

Fig. 4 presents the PL spectra of pure ZnO and Eu, Tb co-deposited ZnO. The photoluminescence spectra of samples were recorded over the wavelength range 300–800 nm with the excitation at 320 nm. All samples exhibited the yellow emission with peak at 580 nm. The yellow emission is related to exciton transition between photo accelerated electrons and charged oxygen vacancy in valence band of ZnO nanoparticles. It could be seen from photoluminescence spectra that the yellow emission with Eu and Tb co-deposited ZnO decreased relative to pure ZnO, indicating the decreased electron-hole recombination, which can accordingly improve the photocatalytic performance of photocatalysts. There is no evidence of emission intensity regarding Eu or Tb, suggesting that Eu^{3+} and Tb^{3+} ions are successfully substituted by Zn^{2+} ions, in agreement with XRD results. Consequently, it was found from photoluminescence data that the simultaneous introduction of Eu and Tb are very effective for the suppression of electron-hole recombination [22].

3.6. XPS analysis

XPS study was used to analyze the elemental composition and chemical states of pure ZnO and ETZ photocatalysts as shown in Fig. 5. The surface composition of Eu, Tb, C, O and Zn was investigated by employing Eu 4d, Tb 4d, C 1S, O 1S and Zn 2p XPS spectra, respectively. The Zn 2p spectra for pure ZnO and ETZ2 resolves into doublet Zn $2p_{3/2}$ and Zn $2p_{1/2}$ peaks centered at 1021.65 and 1044.62 eV binding energies for pure ZnO and 1022.15 and 1045.21 eV for ETZ2 photocatalyst, respectively [23–25]. These two convoluted remarkable Zn 2p peaks confirm the formation of hexagonal wurtzite ZnO [26]. The binding energy difference between these two peaks is 23.06 eV, very well matched with standard value (22.97 eV) indicating the existence of Zn^{2+} ions. A slight shift in Zn 2p peaks towards higher binding energy value and reduction in peak intensity can be clearly observed for ETZ2 photocatalyst compared to that of pure ZnO, which can be assigned to electron transfer between dopants (Eu^{3+}, Tb^{3+}) and ZnO or presence of excess Zn in pure ZnO compared to ETZ2 [13]. The C 1S spectra was used to detect the presence of contaminated CO_2 and deconvoluted into four peaks centered at binding energy values of 289.2, 288.1, 286.4 and 284.6 eV, which could be assigned to COOH, C = O, C–OH and C–C states, respectively [27]. O 1S spectra were deconvoluted into three peaks centered at binging energy 529.61, 531.71 and 533.01 eV employing oxygen in three chemical states, consistent with documented literature. The peak centered at 529.61 eV was attributed to lattice oxygen [28], while peak observed at 531.71 eV attributed to chemisorbed oxygen species [29]. The peak centered at 533.01 eV was accredited to oxygen deficient regions in ZnO lattice. The intensity of this peak indicates the difference in number of oxygen vacancies, may be generating due to defects in ZnO nanoparticles. A small shift of binding energies for ETZ2 as compared to pure ZnO was possibly due to generation of Eu–O bond and Tb–O bonds or transfer of electron between dopants and Zn [28–30]. The XPS spectra of Eu (Tb) 3d was confusing to some extent due to hybridization of Eu 4f orbital (and Tb 4f orbital) with ligand orbital and fractional possession of the valence 4f orbital. XPS spectra of Tb were fitted into two peaks centered in range of 1240.81–1249.36 eV and 12.66 34–1278.27 eV binding energy values for $Tb3d_{3/2}$ and $Tb3d_{5/2}$, respectively. The peaks centered at binding energy values of 1242.56 eV and 1267.16 eV was assigned to Tb^{3+} oxidation state, while peaks centered at 1248.12 eV and 1277.43 eV corresponds to Tb^{4+}oxidation state [15]. Similarly the fitted characteristics peaks of Eu were also deconvoluted into two peaks in the range of 1133.16–1136.79 eV and 1161.32–1165.57 eV binding energy values for $Eu3d_{3/2}$ and $Eu3d_{5/2}$, respectively. The peaks located at binding energy values of 1133.76 eV and 1163.21 eV were assigned to Eu^{3+} oxidation state while peaks situated at 1334. 14 eV and 1164.79 eV were attributed to Eu^{4+} oxidation states. Thus it is concluded that Eu and Tb were found in two oxidation states (3 +, 4 +) in

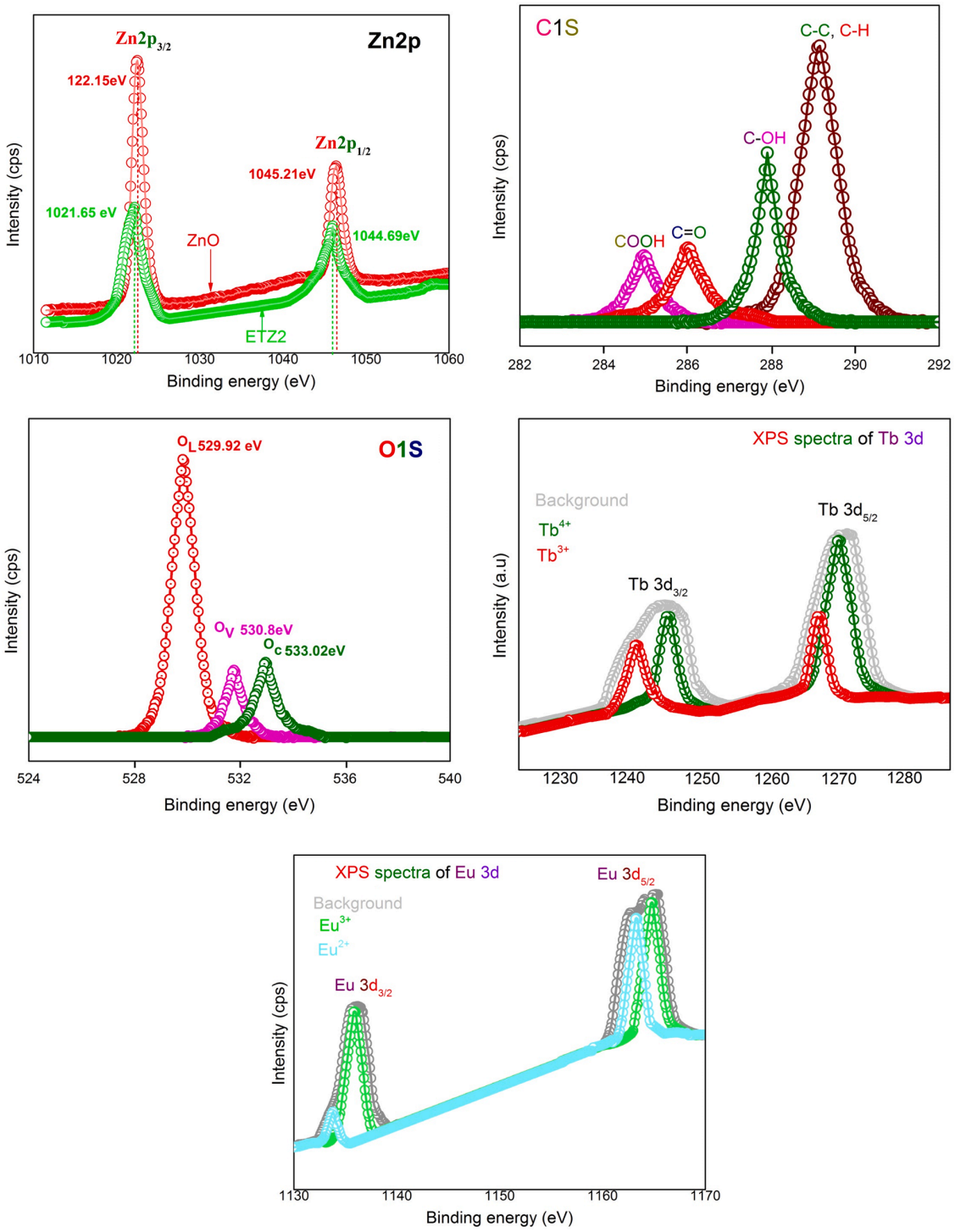

Fig. 5. XPS spectra of ZnO and ETZ photocatalysts.

ZnO photocatalyst [30]. The present XPS results illustrate the simultaneous presence of good amount of carbon and oxygen species in Eu and Tb co-doped ZnO materials.

3.7. Photocurrent and EIS measurements

In order to gain insight into the electronic interaction among dopants and ZnO, the photocurrent transient response of as-prepared various catalysts were also performed in three-electrode system with Pt as the cathode at 0 V vs. Ag/AgCl under visible light illumination. Fig. 6**a** shows the fast photocurrent responses for each switch-on and switch-off operation for ETZ2, ETZ1, TZO, EZO and ZnO catalysts, respectively. It is interesting that the photocurrent of the ETZ2 catalyst is about seven times as high as that of the pure ZnO catalyst. Moreover, the photocurrent is so unstable that obvious photocurrent decay can be found. In contrast, the photocurrent densities of the EZO catalyst exhibit much lower than that of samples contained co-doped ZnO samples (EZT1, ETZ2), suggesting that the introduction of Eu and Tb

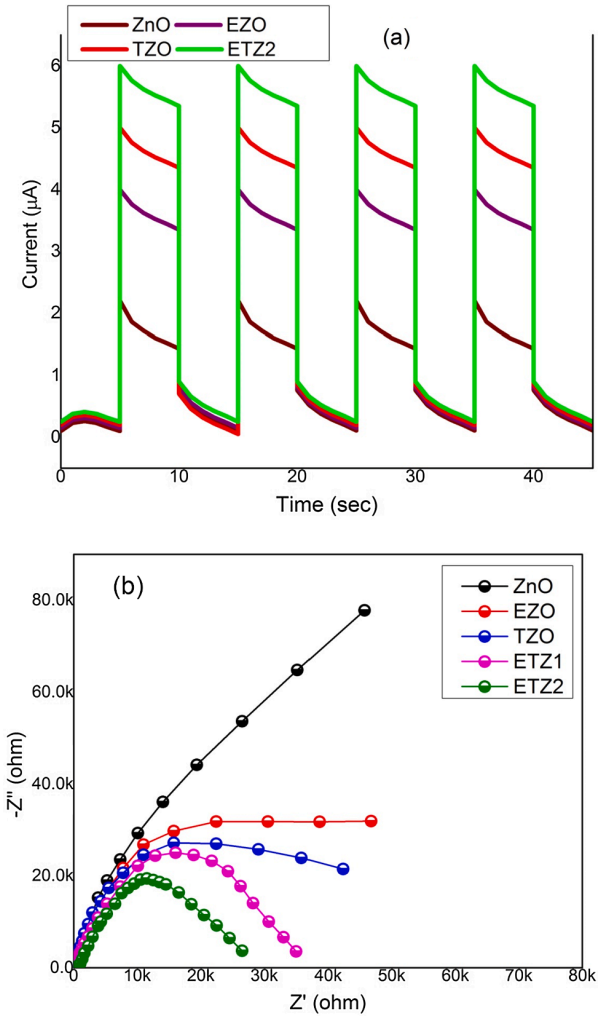

Fig. 6. (a) Photocurrent response of ZnO and doped ZnO (b) EIS Nyquist plot of ZnO and doped ZnO photocatalysts.

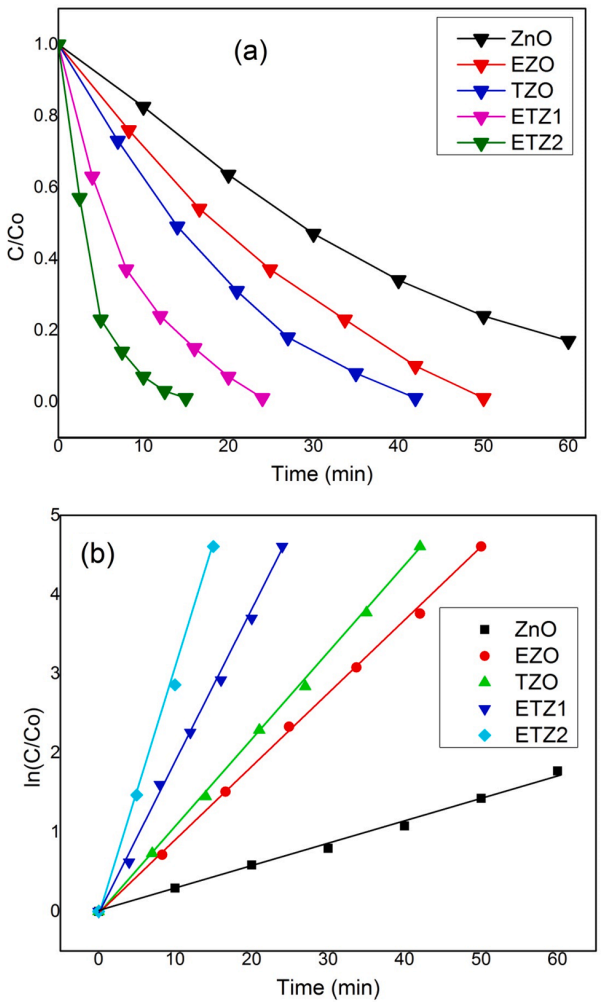

Fig. 7. (a) influence of catalyst with different molar ratio on degradation of MB (catalyst 1 g L^{-1}, MB mg L^{-1}, pH acidic) (b) Kapp order by Langmuir Hinshelwood model.

nanoparticles can be in favor of strengthening the charge separation and transport. In addition, the photocurrent density of ETZ1 and ETZ2 catalysts is also much higher than that of the TZO, which was attributed to the synergistic effect of Eu and Tb in ZnO [31,32]. Fig. 6b EIS was used to examine the as-prepared ZnO and doped ZnO under visible light illumination to obtain insight into the photoactivity of the prepared catalysts. The interface charge separation efficiency of the photo generated electrons and holes are a crucial factor for the photocatalytic activity. The interface charge separation efficiency can be examined by the EIS Nyquist plots. Fig. 6b shows the EIS Nyquist plots of ZnO, EZO, TZO, ETZ1 and ETZ2 under visible light illumination. The arc radius of the EIS Nyquist plot of the doped ZnO was smaller than that of pure ZnO in visible light illumination. Because the arc radius in the EIS spectra reflects the interface layer resistance occurring at the surface of the electrode, more effective separation of photo generated electron-hole pairs and faster interfacial charge transfer occurred on the doped ZnO photocatalyst under this condition. These results clearly show that the interaction of Eu, Tb and ZnO could effectively enhance the separation and transfer efficiency of the photo generated electron-hole pairs in ETZ2 catalyst [33].

4. Photoactivity

4.1. Photocatalytic degradation of MB dye

The photocatalytic degradation of MB was selected to evaluate the photocatalytic activity of pure ZnO, EZO, TZO and ETZ catalysts by using the characteristic absorption values at 642 nm. The reference experiment revealed no degradation of MB in the presence of light but without catalyst. However, a little degradation of MB was noticed in the presence of catalyst but without light illumination, attributed to adsorption of MB on the photocatalyst surface. Thus both light source and catalyst are essential for effective degradation of MB. To quantitatively analyze the photodegradation behavior, the degradation efficiency (C/C_0) of different catalysts was investigated. The photocatalytic performance of pure ZnO sample is unpropitious, affording only 83% degradation of MB under visible illumination after 60 min as shown in Fig. 7**a**. However, the introduction of Eu into ZnO accelerates the photodegradation of MB, certifying that integrating ZnO nanoparticles with RE metals is promising to improve the degradation efficiency. Compared with pure ZnO catalyst, the sample EZO has the degradation efficiency about 99.9% after illumination for 50 min, whilst the efficiency for sample TZO reaches nearly 100% only after 42 min. In contrast, the degradation of nearly 100% occurred within 24 and 15 min for ETZ1 and ETZ2, respectively as shown in Fig. S3. Obviously,

the degradation efficiency for ETZ nanoparticles prepared by the combustion method is much higher than that for EZO, TZO and pure ZnO. The kinetics of the photodegradation of different catalysts is explored to further understand the improved photocatalytic efficiency in the above photocatalysis.

The famous Langmuir-Hinshelwood model is generally used to explain the kinetics of photodegradation of dyes in aqueous dispersion, given as follows [15,16].

$$r = -\frac{dC}{dt} = kr\frac{kaC}{1 + kaC} \tag{2}$$

where ka and kr are adsorption equilibrium and intrinsic rate constants, respectively whilst t is reaction time, C is MB concentration and r represents the degradation rate of MB. When C and ka are very small then factor kaC can be ignored, resulted to first order kinetics

$$r = -\frac{dC}{dt} = k_{app}C \tag{3}$$

When t = 0 and C = C_0 are the quantitative amounts of MB after attaining adsorption-desorption equilibrium, Eq. (2) can be written as

$$ln\frac{Co}{C} = k_{app}t \tag{4}$$

Apparent pseudo first order rate constant Kapp is used as fundamental kinetic factor for synthesized photocatalysts. The slope of linear graph between ln C_0/C and light illumination time 't' would give the kapp. Fig. 7b shows that kapp follows the pseudo first order

ETZ2 (k_{app} = 0.331 min^{-1}) > ETZ1 (k_{app} = 0.143 min^{-1}) > TZO (k_{app} = 0.083 min^{-1}) > EZO (k_{app} = 0.076 min^{-1}) > ZnO (k_{app} = 0.029 min^{-1})

For EZO and TZO, the k value is about 3 and 4 times higher than pure ZnO nanoparticles, respectively. In particular, the ETZ2 sample shows highest value of the rate constant, which is almost 11.4 times greater than ZnO nanoparticles. Herein, it can be directly observed that the photodegradation efficiency of ETZ2 is much higher than that of pure ZnO nanoparticles owing to faster separation efficiency of photo induced electrons and holes in ETZ catalysts.

4.1.1. Influence of operational parameters on photo-decomposition of MB dye

The photocatalyst tests evaluated at various loading amount (0.25–2.5 g L^{-1}) to optimize the catalyst dose, revealed that photodegradation rate of MB dye increases with enhance in catalyst dose from 0.25 to 1.5 g/L and then degradation of MB dye reduces as shown in Fig. S4. The primary increase in the degradation rate may be ascribed to enhance in surface area, the presence of more active sites on photocatalyst surface and increased penetration of absorbed light. However, the decrease in degradation rate beyond 1.5 g/L can be attributed to suppressed light penetration and reduced surface area due to agglomeration, results in decreased number of light photons reaching the active surface sites [35,36].

The pH of the reaction mixture plays an important role in the degradation of dyes because it determines the surface charge properties of the catalyst, adsorption/desorption of dyes on the surface of the catalyst, and charges on the dye molecules. Therefore, it is important to study the degradation of dyes at varying pH values of the reaction mixture. In order to see the role of pH on the degradation of MB, we performed experiments at different pH values varying from 5 to 11 using ETZ2 catalyst. The pH of the reaction mixture was maintained before illumination by adding an aqueous solution of either HNO_3 or NaOH. It could be seen from Fig. 8 that the decomposition of MB dye increases upon increases in pH from 5 to 9 and a further increase in pH leads to a decrease in MB degradation. The rate of decomposition of dye depends on the adsorption of dyes on the surface of ZnO nanoparticles. However, adsorption of dyes depends upon the ionic structure of dyes and point charge value of ZnO. Since the zero point charge for doped

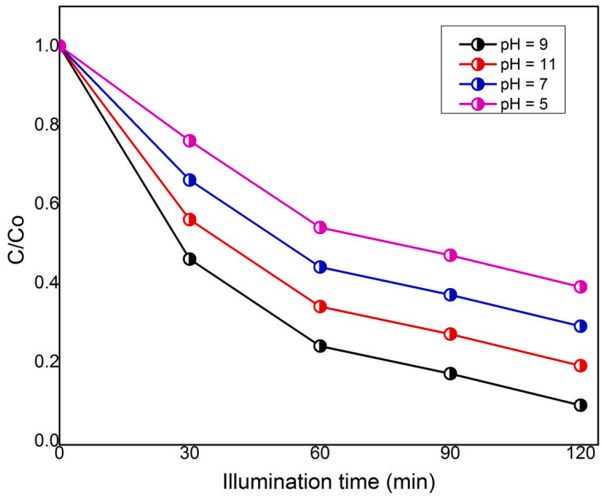

Fig. 8. Influence of initial pH on MB degradation (ETZ2 catalyst 1 g L^{-1}, MB 10 mg L^{-1}).

ZnO (pHzpc) is about 8.8. The surface of the catalyst remains positively charged below pHzpc whereas the catalyst surface is negatively charged above pHzpc, according to Eqs. (8) and (9), respectively [34].

$$Zn - OH + H^+ \rightarrow Zn - OH_2^+ (pH<pH_{PZC} \tag{5}$$

$$Zn - OH + OH^- \rightarrow Zn - O^- + H_2O (pH>pH_{PZC} \tag{6}$$

The results revealed that the photodegradation of MB dye increases with enhancing solution pH from 5 to 9 and further enhance in pH leads to reduced decomposition of MB dye. The maximum degradation efficiency is observed at pH 9, attributed to better interaction of MB molecules with surface of the photocatalyst at this pH value. The decrease in degradation at pH 11 may be attributed to dissolution of ZnO nanoparticles as indicated in following equations [37–39].

$$ZnO + 2h^+ \rightarrow Zn^{+2} + \frac{1}{2}O_2 \tag{7}$$

$$ZnO + 2H^+ \rightarrow Zn^{+2} + 2H_2O \tag{8}$$

$$ZnO + H_2O + 2OH^- \rightarrow Zn(OH)_4^{-2} \tag{9}$$

4.1.2. Mechanism of MB degradation

On absorption of photons of energy equal to or greater than the band gap of the prepared ZnO nanoparticles, an electron can be excited from the VB to the CB leaving behind a hole (h^+). Generally, the photocatalytic degradation of dye in the presence of pure ZnO was found to be less than ETZ catalysts due to the recombination of charge carriers. The enhanced photocatalytic activity of ETZ catalysts is not only due to the fact that dopants can improve the absorption efficiency of the nanoparticles to illumination light, but they also inhibit the recombination rate of charge carriers by trapping the electron, which improved the separation of the electron and hole. Furthermore, the higher separation of electron and hole by ETZ catalyst was confirmed by PL spectra. The trapped electron is picked up by oxygen to generate superoxide radical anions. At the same time the hole generated at the VB may react with surface bound H_2O to produce the highly reactive hydroxyl radical [40]. The superoxide radical anions ($*O2^-$) and hydroxyl radicals (*OH) produced under visible light illumination are responsible for the degradation of dye. In addition, ETZ have a small crystallite size and therefore possess a large surface area as inferred from BET, SEM and XRD. Photocatalytic activity also depends upon surface area; a larger surface area provides higher activity due to increased adsorption area. Hence, the hexagonal ETZ nanoparticles provide efficient photocatalytic activity [41]. On the other hand a dye-

sensitized mechanism may also be possible as indicated in experiments carried out for degradation of dye over pure ZnO nanoparticles under a visible light source. MB dye is also visible light absorbing and get excited in visible light. The excited dye* can transfer the electron to the conduction band of ZnO nanoparticles [42–44]. The electron can be trapped by the dopant at the surface or by the impurity band preventing the recombination rate of the charge carrier. The trapped electrons may subsequently be transferred to adsorbed oxygen to generate the superoxide radical anion ($*O2^-$) which may act as a strong reducing agent and may form hydrogen peroxide as indicated in the following equations [45,46]. The hydroxyl radical (*OH) formed in the reaction mixture may act as a strong oxidizing agent.

$$Dye + visiblelight \rightarrow dye^* \quad (10)$$

$$ETZ \xrightarrow{h\tilde{N}} e_{CB}^- + h_{VB}^+ \quad (11)$$

$$dye^* + \mathrm{ETZ} \rightarrow dye^{*+} + e_{CB}^- \quad (12)$$

$$Eu/Tb^{+4} + O_2 \rightarrow Eu/Tb^{+3} + O_2^{*-} \quad (13)$$

$$e_{CB}^- + O_2 \rightarrow O_2^{*-} \quad (14)$$

$$h_{VB}^+ + H_2O \rightarrow *_{OH} + H^+ \quad (15)$$

$$O_2^{*-} + H_2O + 2H^+ \rightarrow H_2O_2 + O_2 \quad (16)$$

$$H_2O_2 + e^- \rightarrow *_{OH} + -_{OH} \quad (17)$$

$$O_2^{*-}/\ *_{OH} + absrobeddye/dye^{*+} \rightarrow degradationproducts \quad (18)$$

4.2. Photocatalytic H_2 generation

4.2.1. Influence of light illumination time on catalyst

All the synthesized catalysts were evaluated for hydrogen generation under visible light illumination. A reference experiment revealed no hydrogen generation in the absence of either photocatalyst or illumination source, identifying both photocatalyst and illumination source are essential for photocatalytic activity. The wide band gap of ZnO makes it inactive for H_2 generation under visible light illumination, whereas all modified catalysts considerably harvest visible light and revealed optimistic result towards H_2 generation activity under visible light illumination as shown in Fig. 9.. It can be observed that the quantity of H_2 generation all enhance gradually with lengthening the light illumination time for synthesized photocatalyst. The photocatalytic hydrogen generation was in the order of ETZ2 (144 μmol) > ETZ1 (131 μmol) > TZO (112 μmol) > EZO (103μol) > ZnO (22 μmol) at 0.2 wt% loading content under 6 h visible light illumination. It is convincing since by increasing the visible light illumination time the number of photo generated charge carriers on ZnO will enhance, consequently increasing the hydrogen generation activity. The maximum hydrogen generation rate of ETZ2 catalyst with all lengthening time is ascribed to the formation of more active sites to trap more charge carriers due to introduction of highest content of Eu^{3+} and Tb^{3+} ions [49].

4.2.2. Influence of catalyst loading content on photocatalytic H_2 generation

Fig. S5 shows the influence of catalyst dose with different loaded amounts on photocatalytic activities of ZnO and doped ZnO photocatalysts. It can be remarked that, for these catalysts, their photocatalytic activities all increase with the increase in the catalyst loading contents, but only when the loaded amounts are below 0.20 wt%. And then, they decrease with the further increase in the loading contents when they are higher than their corresponding maximum values in each case. Of course, the higher contents of the loaded catalysts are apparently detrimental to the enhancement of the photocatalytic activity [49,50]. The amount of hydrogen generation under 6 h visible light illumination at 0.20 wt% catalyst loadings are 18.6, 186, 234, 397.2 and 533.8 μmol for pure ZnO, EZO, TZO, ETZ1 and ETZ2 catalysts, respectively. This is expected because catalysts clusters highly dispersed at a lower concentration act as a separation center and a sink for photo generated electrons [51]. Hence, the photo generated electrons and holes are efficiently separated. However, the catalysts clusters at a higher concentration may work as a recombination center and the recombination rate between electrons and holes will increase exponentially with the increase in loading concentration, because the average distance among trapping sites decreases by increasing the number of the clusters confined within a particle.

4.2.3. Influence of initial pH value on photocatalytic H_2 generation

The role of initial pH (5–11) on photocatalytic hydrogen generation was evaluated using methanol as sacrificial agent, noting that initial pH of the original solution containing 200 mL distilled water and 10 mL methanol (2.25 M) is 8.8 and insignificant changes of solution pH were observed after the course of photocatalytic reactions. Fig. 10 depicts that photocatalytic hydrogen generation increases with enhance in initial solution pH from 5 to 9 and then hydrogen generation efficiency remarkably reduces with further enhance in initial solution pH. The results reveal that mild acidic conditions induce higher hydrogen generation efficiency of ETZ photocatalysts under visible light illumination and the optimum solution pH is 9. The pH_{pzc} for ZnO is approximately

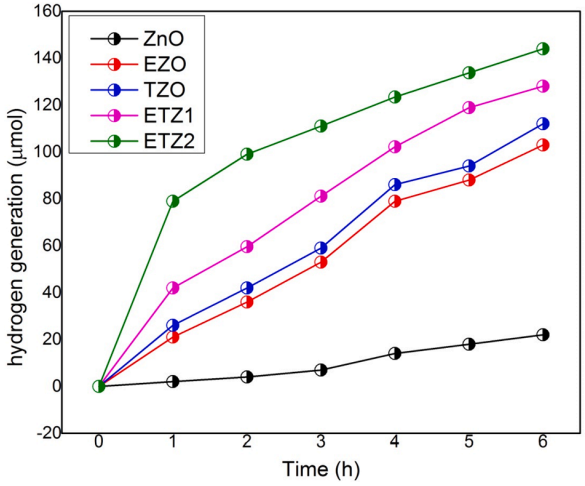

Fig. 9. Influence of visible light illumination time on photocatalytic hydrogen generation.

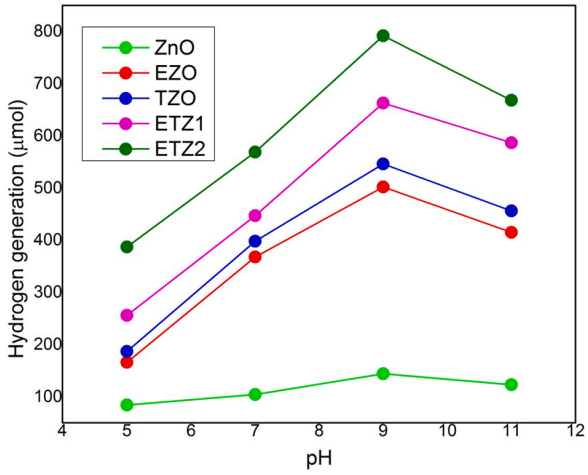

Fig. 10. Influence of initial pH value on photocatalytic H_2 generation under visible light illumination.

at pH 8.6–9.0[52]. At pH = pH_{pzc}, when photocatalyst contains no charge, the species/molecules are probably allowed to much more easily reach the photocatalyst surface and achieve higher photocatalytic reaction activity [53,54], thus experimentally obtaining the highest H_2 generation activity at the initial solution. The photocatalytic hydrogen generation was in the order of ETZ2 (792 μmol) > ETZ1 (663 μmol) > TZO (546 μmol) > EZO (502 μmol) > ZnO (64 μmol) at pH = 9. The initial solution pH of 9 can significantly enhance the hydrogen generation rate of ETZ2 catalyst almost eleven times as the hydrogen generation of pure ZnO.

4.2.4. Mechanism

The photocatalytic mechanism of the ETZ photocatalysts under visible light illumination can be explained as follows: Tb^{4+} and Eu^{2+} are half-filled in the 4*f* orbital that holds 7 *f*-electrons, and this configuration is relatively stable. In this case, Eu^{3+} could not effectively capture the photo-generated electrons on the surface of the ETZ catalysts because the PL intensities of ETZ was just decreased a little bit compared with pure ZnO. Therefore, the photo-generated electrons in ETZ were trapped by the Tb^{4+} ions, forming Tb^{3+}. Then the Eu^{3+} were reduced by the formative $Tb3^{+}$ to generate a reduction species Eu^{2+}, and the Tb^{3+} returned to their original stable half-filled stable (Tb^{4+}), while valence band holes react with surface H_2O molecules to generate H^+ ions and *OH radicals [55,56]. Eu^{+2}/Tb^{+3} can react with *OH to produce Eu^{+3}/Tb^{+4} and OH^-. H^+ can attain the conduction band electrons of ZnO to generate the H_2 gas. Ultimately, the reduction species Eu^{2+}/Tb^{+3} could easily reduce the *OH radical on the surface of the ETZ catalysts to form OH^-, so the Eu^{2+}/Tb^{+3} could be oxidized back to Eu^{3+}/Tb^{+4} [57]. As a result of the recycle reactions, the twice-cycled trapping and releasing process of electrons tremendously reduced the recombination rate of electron-hole pairs, which contributed to hydrogen generation. Ultimately H^+ ions reduce to H_2. Therefore, unlike the typical transition metal-doped semiconductors for photocatalysis where the dopants introduce more recombination centers to consume the charge carriers, Tb/Eu co-doping in ZnO results in the generation of in-built $Tb^{4+/}Tb^{3+}$ and Eu^{3+}/Eu^{2+} pairs that act as redox cycles to immensely facilitate charge separation and restrain recombination.

Meanwhile, keeping in mind the standard redox-potential values of Eu^{+2}/Tb^{+3} and Eu^{+3}/Tb^{+4} (Eu^{+2}/Tb^{+3} = −0.36 V, Eu^{+2}/Tb^{+3} = −0.38 V), the main reaction was considered as

$$Tb^{+4} + e^-_{CB} \rightarrow Tb^{+3} \quad (19)$$

$$Tb^{+3} + Eu^{+3} \rightarrow Tb^{+4} + Eu^{+2} \quad (20)$$

$$h^+ + H_2O \rightarrow OH^* + H^+ \quad (21)$$

$$Eu^{+2}/Tb^{+3} + OH^* \rightarrow OH^- + Eu^{+3}/Tb^{+4} \quad (22)$$

$$2H^+ + e^- \rightarrow H_{2(g)} \quad (23)$$

4.3. Photocatalytic CO_2 reduction

To evaluate the photoreduction activities of as-prepared pure and doped ZnO materials, photocatalytic CO_2 reduction with water vapor was conducted at ambient temperature and atmospheric pressure. The performance of the as-synthesized photocatalysts was studied under visible light. The experiment was performed without both light illumination and photocatalyst. In these cases, negligible carbon related products were detected. This showed that the product yields stemmed from photocatalytic reduction of CO_2 and highlighted the significance of the photocatalyst and light source to drive the reaction. Fig. 11**c** shows the total production of CH_4 over pure and doped ZnO after 6 h of reaction under visible light illumination. As illuminated by the results, pure ZnO exhibited minimal production of CH_4, with a total yield of 1.35 μmol g^{-1}. It is remarkable fact that, the variation tendency of CH_4 yield for EZO and TZO is strikingly different with that of ZnO. The yield of EZO and TZO is 2.2 and 2.5 μmol g^{-1}, which are 1.4 and 1.85 times than that of pure ZnO, respectively. When it comes to ETZ2, the variation of CH_4 yield 4.59 μmol g^{-1}, which was 3.4 fold higher in comparison to pure ZnO. Therefore, the appropriate Eu and Tb co-addition markedly enhancing CH_4 yield finally. The photocatalytic enhancement of Eu and Tb co-doped ZnO was accredited to several concomitant factors. Firstly, the presence of oxygen deficient surface defects significantly alters the optical properties of ZnO, which guarantees enhanced light absorption to promote electron hole pair generation, along with band gap narrowing [58]. In addition, surface defects created due to dopants played an indispensable role to trap photo induced electrons, hence improving the electron hole pair separation and inhibiting the direct recombination of photogene rated charge carriers as confirmed by PL spectra. Secondly, high specific surface of resulting RE doped ZnO photocatalysts favors surface capture of CO_2 molecules, which is the prerequisite step for the following photocatalytic reduction steps [59].

According to published literature electron in the conduction band minima can oxidize water molecules giving rise to O_2 and protons. Due to lower valence band minima (VBM) position the rate for O_2 generation for catalyst will improve, indirectly leading to enhance the CO_2 photo reduction rate. On the other hand, the electron on the conduction band minima (CBM) can reduce adsorbed CO_2 molecules to CH_4 under the assistance of the protons [47,48,60]. The above photo catalytic reactions mainly depend on three parameters: (1) light absorption of catalysts, (2) migration of charge carriers, and (3) use of the charge carriers in the processes. In our experiment, the adsorption of light is increased and the PL intensity is decreased after Eu and Tb co-modification, which indicates the co-modified catalyst, has increased capacity of light adsorption and longer lifetime of charger carriers. Changes of two general aspects are favorable for increased photocatalytic conversion of CO_2 to CH_4. Considering the results of FTIR, it is found that the capacity of CO_2 adsorption is enhanced notably. We conclude that the photocatalytic reaction rate for CO_2 reduction on the pure ZnO catalyst is slow due to the limited CO_2 adsorption on the catalyst surface. In other words, if there is no enough CO_2 adsorption on the surface of catalysts, the following process of C–O bond breaking and C–H bond formation is impossible to complete. It is reasonable that the CO_2 adsorption on surface of Eu and Tb co-modified ZnO is rate determining step in the process of CO_2 to CH_4.

A possible mechanism for photocatalytic CO_2 under visible light illumination can be explained as follows: the electrons are transferred to conduction band leaving holes behind in the valence band. The holes on the valence band minima oxidize water molecules to produce oxygen and protons. On the other hand, electrons on conduction band minima can reduce adsorbed CO_2 molecule to CH_4 with support of protons. The mechanism of CO_2 is given as follows: The oxidation reaction on the valence band minima is

$$2H_2O + 4h^+ \rightarrow O_2 + 4H^+ \quad (24)$$

The reduction reaction on conduction band minima is

$$CO_2 + 8H^+ + 8e^- \rightarrow CH_4 + 2H_2O \quad (25)$$

The overall reaction will be

$$H_2O + CO_2 \rightarrow O_2 + CH_4 \quad (26)$$

4.3.1. Stability tests

In all the environmental remedial processes, stability of the materials is a key factor. Although, research has been varied out on the photocatalytic performances of ZnO and ZnO based materials, but stability mechanism are limited. In present work, the performance of the ZnO on successive recycling under the influence of visible light illumination was evaluated and shown in Fig. 11**a**. In the presence of visible light (Fig. 11a), no significant change in the degradation was observed for four consecutive cycles and the degradation percentage decreased from 100% to 96% after four cycles indicating nearly stable

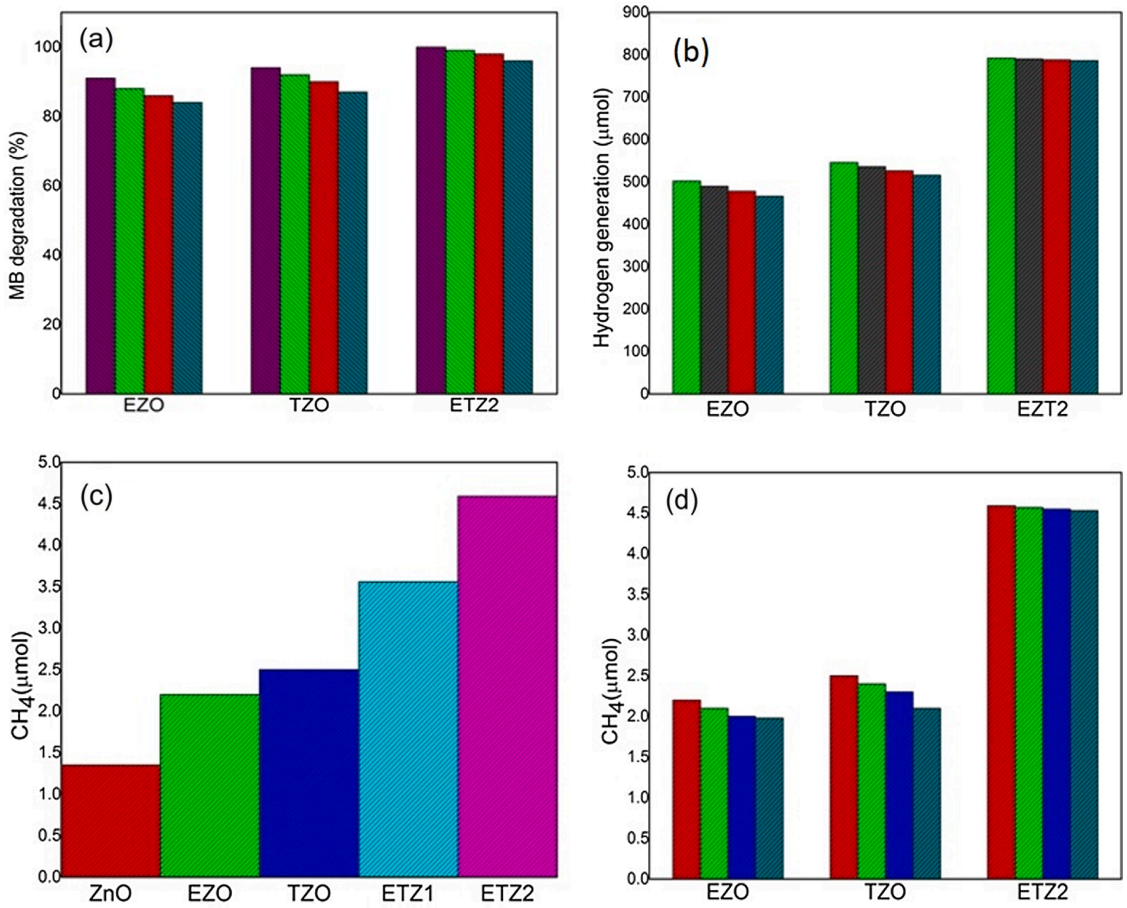

Fig. 11. Stability of photocatalysts with four successive cycles (a) MB degradation (b) H_2 generation (d) CO_2 reduction (c) CO_2 reduction of ZnO and doped photocatalysts.

activity. A constant decreasing trend was observed for TZO and EZO catalysts in the presence of visible light. The photodegradation percentages are 94% and 91% (1st run), 92% and 88% (2nd run), 90% and 85% (3rd run) and87% and 84% (4th run) for TZO and EZO, respectively. This decrease in trend could be attributed to the photocorrosion on the surface of ZnO due to the holes participation that destroys the structure of ZnO.

ETZ2 catalyst showed 98% stability during four consecutive H_2 generation cycles as shown in Fig. 11**b**. TZO sample showed strong stability during first two run and a slightly decreased stability (94%) during next two successive run comparing to the ETZ2 sample, indicating that sample can be stable for certain period of time while the long term stability of the present TZO photocatalyst would still need to be improved for future applications. Similarly, EZO catalyst showed obvious continuous loss of activity during the whole reaction, ultimately showing 92% stability after four consecutive run.

It is clear that the ETZ2 catalyst remained stable for the photocatalytic reduction of CO_2 with H_2O after running four cycles under experimental condition as shown in Fig. 11**d**. The stability rate of CH_4 was observed to be 84% and 90% for EZO and TZO, respectively.

4.4. Conclusion

In summary, we have successfully synthesized Eu and Tb co-doped ZnO materials via facile and inexpensive combustion method for diverse photocatalytic applications. These materials were characterized by XRD, SEM, EDS, BET, FTIR, UV–visible DRS, PL, XPS and EIS and their photocatalytic activities for MB degradation, hydrogen generation and CO_2 reduction were evaluated under visible light illumination. The 100% MB degradation under visible light illumination reported for EZO and TZO catalysts was obtained within 50 and 42 min, respectively and Eu and Tb co-doping of 3 mol% (ETZ2) showed the 100% MB degradation in just 15 min under visible light illumination. The ETZ2 photocatalyst also obtained the highest hydrogen generation of 144, 538.8 and 792 µmol among all synthesized catalysts as a function of visible light illumination time, catalyst dose and initial solution pH, respectively. The photocatalytic performance of as obtained samples indicates that introduction of Eu and Tb dopants to ZnO can effectively increases the catalytic process of CH_4 yield 4.59 µmol g^{-1}, which was 3.4 fold higher in comparison to pure ZnO. Combining the photocatalytic results, introduction of Eu and Tb can greatly improve the formation of Eu^{+2}/Eu^{+3} and Tb^{+3}/Tb^{+4} mixed valence states, surface defects and oxygen vacancies. Thus, Eu and Tb co-doped ZnO nanoparticles have applications in the fields of photocatalytic degradation of extensive organic pollutants, photocatalytic water splitting hydrogen generation and CO_2 reduction. Hence, precisely designed Eu and Tb doped ZnO architectures are expected to provide new avenues for the development of high performance photocatalysts having applications in hydrogen energy and environmental abatement.

Declaration of Competing Interest

All authors declare that they do not have any conflict of interest statement.

Appendix A. Supplementary material

Supplementary data to this article can be found online at https://doi.org/10.1016/j.seppur.2019.116328.

References

[1] J. Zhao, Y. Ding, J. Wei, X. Du, Y. Yu, R. Han, A molecular Keggin polyoxometalate catalyst with high efficiency for visible-light driven hydrogen evolution, Int. J. Hydrogen Energy 39 (33) (2014) 18908–18918.

[2] Y.P. Yuan, S.W. Cao, L.S. Yin, L. Xu, C. Xue, NiS_2 co-catalyst decoration on $CdLa_2S_4$ nanocrystals for efficient photocatalytic hydrogen generation under visible light irradiation, Int. J. Hydrogen Energy 38 (18) (2013) 7218–7223.

[3] X. Shi, K. Zhang, J.H. Park, Understanding the positive effects of (CoePi) co-catalyst modification in inverse-opal structured a-Fe_2O_3-based photoelectrochemical cells, Int. J. Hydrogen Energy 38 (12725) (2013) e12732.

[4] J.H. Kim, G. Magesh, H.J. Kang, M. Banu, J.H. Kim, J. Lee, J.S. Lee, Carbonate-coordinated cobalt co-catalyzed $BiVO_4/WO_3$ composite photoanode tailored for CO_2 reduction to fuels, Nano Energy 15 (2015) 153–163.

[5] M.M. Alnuaimi, M.A. Rauf, S.S. Ashraf, Comparative decoloration study of Neutral Red by different oxidative processes, Dyes Pigm. 72 (3) (2007) 367–371.

[6] A. Mantilla, F. Tzompantzi, J.L. Fernández, J.D. Góngora, G. Mendoza, R. Gómez, Photodegradation of 2, 4-dichlorophenoxyacetic acid using ZnAlFe layered double hydroxides as photocatalysts, Catal. Today 148 (1–2) (2009) 119–123.

[7] W. Cun, Z. Jincai, W. Xinming, M. Bixian, S. Guoying, P. Pingan, F. Jiamo, Preparation, characterization and photocatalytic activity of nano-sized ZnO/SnO_2 coupled photocatalysts, Appl. Catal. B 39 (3) (2002) 269–279.

[8] S. Liu, C. Li, J. Yu, Q. Xiang, Improved visible-light photocatalytic activity of porous carbon self-doped ZnO nanosheet-assembled flowers, CrystEngComm 13 (7) (2011) 2533–2541.

[9] W.J. Sun, J. Li, G. Mele, Z.Q. Zhang, F.X. Zhang, Enhanced photocatalytic degradation of rhodamine B by surface modification of ZnO with copper (II) porphyrin under both UV–vis and visible light irradiation, J. Mol. Catal. A: Chem. 366 (2013) 84–91.

[10] Y. Min, K. Zhang, Y. Chen, Y. Zhang, W. Zhao, Synthesis of nanostructured ZnO/Bi_2WO_6 heterojunction for photocatalysis application, Sep. Purif. Technol. 92 (2012) 115–120.

[11] P. Malathy, K. Vignesh, M. Rajarajan, A. Suganthi, Enhanced photocatalytic performance of transition metal doped Bi_2O_3 nanoparticles under visible light irradiation, Ceram. Int. 40 (1) (2014) 101–107.

[12] B.M. Rajbongshi, S.K. Samdarshi, Cobalt-doped zincblende–wurtzite mixed-phase ZnO photocatalyst nanoparticles with high activity in visible spectrum, Appl. Catal. B 144 (2014) 435–441.

[13] I.N. Reddy, C.V. Reddy, J. Shim, B. Akkinepally, M. Cho, K. Yoo, D. Kim, Excellent visible-light driven photocatalyst of (Al, Ni) co-doped ZnO structures for organic dye degradation. Catalysis Today (2018).

[14] Phuruangrat, A., Yayapao, O., Thongtem, T. and Thongtem, S., 2014. Synthesis and characterization of europium-doped zinc oxide photocatalyst. J. Nanomat. (2014).

[15] H.V.S. Pessoni, L.J.Q. Maia, A. Franco Jr, Eu-doped ZnO nanoparticles prepared by the combustion reaction method: structural, photoluminescence and dielectric characterization, Mater. Sci. Semicond. Process. 30 (2015) 135–141.

[16] J. Sowik, M. Miodyńska, B. Bajorowicz, A. Mikolajczyk, W. Lisowski, T. Klimczuk, D. Kaczor, A.Z. Medynska, A. Malankowska, Optical and photocatalytic properties of rare earth metal-modified ZnO quantum dots, Appl. Surf. Sci. 464 (2019) 651–663.

[17] P.V. Korake, A.N. Kadam, K.M. Garadkar, Photocatalytic activity of Eu3 + -doped ZnO nanorods synthesized via microwave assisted technique, J. Rare Earths 32 (4) (2014) 306–313.

[18] M. Salavati-Niasari, J. Javidi, F. Davar, Sonochemical synthesis of Dy2 (CO3) 3 nanoparticles, Dy (OH) 3 nanotubes and their conversion to Dy2O3 nanoparticles, Ultrason. Sonochem. 17 (5) (2010) 870–877.

[19] A. Manikandan, E. Manikandan, B. Meenatchi, S. Vadivel, S.K. Jaganathan, R. Ladchumananandasivam, M. Henini, M. Maaza, J.S. Aanand, Rare earth element (REE) lanthanum doped zinc oxide (La: ZnO) nanomaterials: synthesis structural optical and antibacterial studies, J. Alloy. Compd. 723 (2017) 1155–1161.

[20] K.S. Yu, J.Y. Shi, Z.L. Zhang, Y.M. Liang, W. Liu, Synthesis, characterization, and photocatalysis of ZnO and Er-Doped ZnO, J. Nanomater. 2013 (2013) 75.

[21] L. Zhang, Y. Yang, R. Fan, J. Yu, L. Li, Improving the efficiency of ZnO-based dye-sensitized solar cells by Pr and N co-doping, J. Mater. Chem. A 1 (39) (2013) 12066–12073.

[22] Y. Ling, W. Jiang, X. Wu, X. Bai, Preparation and visible light photocatalytic properties of (Er, La, N)-codoped TiO_2 nanotube array films, J. Nanosci. Nanotechnol. 9 (2) (2009) 714–717.

[23] M. Peres, A. Cruz, S. Pereira, M.R. Correia, M.J. Soares, A. Neves, M.C. Carmo, T. Monteiro, A.S. Pereira, M.A. Martins, T. Trindade, Optical studies of ZnO nanocrystals doped with Eu^{3+} ions, Appl. Phys. A 88 (1) (2007) 129–133.

[24] J. Yang, X. Li, J. Lang, L. Yang, M. Wei, M. Gao, X. Liu, H. Zhai, R. Wang, Y. Liu, J. Cao, Synthesis and optical properties of Eu-doped ZnO nanosheets by hydrothermal method, Mater. Sci. Semicond. Process. 14 (3–4) (2011) 247–252.

[25] D.D. Wang, G.Z. Xing, J.H. Yang, L.L. Yang, M. Gao, J. Cao, Y.J. Zhang, B. Yao, Dependence of energy transfer and photoluminescence on tailored defects in Eu-doped ZnO nanosheets-based microflowers, J. Alloy. Compd. 504 (1) (2010) 22–26.

[26] U. Alam, A. Khan, W. Raza, A. Khan, D. Bahnemann, M. Muneer, Highly efficient Y and V co-doped ZnO photocatalyst with enhanced dye sensitized visible light photocatalytic activity, Catal. Today 284 (2017) 169–178.

[27] A. Rjeb, S. Letarte, L. Tajounte, M.C. El Idrissi, A. Adnot, D. Roy, Y. Claire, J. Kaloustian, Polypropylene natural aging studied by X-ray photoelectron spectroscopy, J. Electron Spectrosc. Relat. Phenom. 107 (3) (2000) 221–230.

[28] H. Yang, J.X. Zhang, G.J. Lin, T. Xian, J.L. Jiang, Preparation, characterization and photocatalytic properties of terbium orthoferrite nanopowder, Adv. Powder Technol. 24 (1) (2013) 242–245.

[29] M. Wegmann, L. Watson, A. Hendry, XPS analysis of submicrometer barium titanate powder, J. Am. Ceram. Soc. 87 (3) (2004) 371–377.

[30] H. Li, W. Li, S. Gu, F. Wang, H. Zhou, X. Liu, C. Ren, Enhancement of photocatalytic activity in Tb/Eu co-doped Bi_2MoO_6: the synergistic effect of Tb–Eu redox cycles, RSC Adv. 6 (53) (2016) 48089–48098.

[31] D.J. Milliron, S.M. Hughes, Y. Cui, L. Manna, J. Li, L.W. Wang, A.P. Alivisatos, Colloidal nanocrystal heterostructures with linear and branched topology, Nature 430 (6996) (2004) 190.

[32] X. Wang, J. Song, Z.L. Wang, Nanowire and nanobelt arrays of zinc oxide from synthesis to properties and to novel devices, J. Mater. Chem. 17 (8) (2007) 711–720.

[33] J. Pan, D. Thierry, C. Leygraf, Electrochemical impedance spectroscopy study of the passive oxide film on titanium for implant application, Electrochim. Acta 41 (7–8) (1996) 1143–1153.

[34] Y.U. Yaoguang, C.H.E.N. Gang, Z.H.O.U. Yansong, H.A.N. Zhonghui, Recent advances in rare-earth elements modification of inorganic semiconductor-based photocatalysts for efficient solar energy conversion: a review, J. Rare Earths 33 (5) (2015) 453–462.

[35] D. Daksh, Y.K. Agrawal, Rare earth-doped zinc oxide nanostructures: a review, Rev. Nanosci. Nanotechnol. 5 (1) (2016) 1–27.

[36] W. Raza, S.M. Faisal, M. Owais, D. Bahnemann, M. Muneer, Facile fabrication of highly efficient modified ZnO photocatalyst with enhanced photocatalytic, antibacterial and anticancer activity, RSC Adv. 6 (82) (2016) 78335–78350.

[37] S. Balachandran, K. Thirumalai, M. Swaminathan, Facile hydrothermal synthesis of a highly efficient solar active Pr_6O_{11}–ZnO photocatalyst and its multiple applications, RSC Adv. 4 (53) (2014) 27642–27653.

[38] S. Chakrabarti, B.K. Dutta, Photocatalytic degradation of model textile dyes in wastewater using ZnO as semiconductor catalyst, J. Hazard. Mater. 112 (3) (2004) 269–278.

[39] Y. Hong, C. Tian, B. Jiang, A. Wu, Q. Zhang, G. Tian, H. Fu, Facile synthesis of sheet-like ZnO assembly composed of small ZnO particles for highly efficient photocatalysis, J. Mater. Chem. A 1 (18) (2013) 5700–5708.

[40] K.J. Kim, P.B. Kreider, C. Choi, C.H. Chang, H.G. Ahn, Visible-light-sensitive Na-doped p-type flower-like ZnO photocatalysts synthesized via a continuous flow microreactor, RSC Adv. 3 (31) (2013) 12702–12710.

[41] S.G. Kumar, K.K. Rao, Zinc oxide based photocatalysis: tailoring surface-bulk structure and related interfacial charge carrier dynamics for better environmental applications, RSC Adv. 5 (5) (2015) 3306–3351.

[42] Y. Liang, N. Guo, L. Li, R. Li, G. Ji, S. Gan, Preparation of porous 3D Ce-doped ZnO microflowers with enhanced photocatalytic performance, RSC Adv. 5 (74) (2015) 59887–59894.

[43] Y. Liang, N. Guo, L. Li, R. Li, G. Ji, S. Gan, Facile synthesis of Ag/ZnO micro-flowers and their improved ultraviolet and visible light photocatalytic activity, New J. Chem. 40 (2) (2016) 1587–1594.

[44] Y. Lu, Y. Lin, T. Xie, S. Shi, H. Fan, D. Wang, Enhancement of visible-light-driven photoresponse of Mn/ZnO system: photogenerated charge transfer properties and photocatalytic activity, Nanoscale 4 (20) (2012) 6393–6400.

[45] P. Wang, T. Dong, C. Jia, P. Yang, Ultraselective acetone-gas sensor based ZnO flowers functionalized by Au nanoparticle loading on certain facet, Sens. Actuat. B 288 (2019) 1–11.

[46] B. Subash, B. Krishnakumar, R. Velmurugan, M. Swaminathan, M. Shanthi, Synthesis of Ce co-doped Ag–ZnO photocatalyst with excellent performance for NBB dye degradation under natural sunlight illumination, Catal. Sci. Technol. 2 (11) (2012) 2319–2326.

[47] C.J. Chang, K.L. Huang, J.K. Chen, K.W. Chu, M.H. Hsu, Improved photocatalytic hydrogen production of ZnO/ZnS based photocatalysts by Ce doping, J. Taiwan Inst. Chem. Eng. 55 (2015) 82–89.

[48] Y.T. Prabhu, V.N. Rao, M.V. Shankar, B. Sreedhar, U. Pal, The facile hydrothermal synthesis of CuO@ ZnO heterojunction nanostructures for enhanced photocatalytic hydrogen evolution, New J. Chem. 43 (17) (2019) 6794–6805.

[49] Y. Zhong, K. Ueno, Y. Mori, T. Oshikiri, H. Misawa, Cocatalyst effects on hydrogen evolution in a plasmon-induced water-splitting system, J. Phys. Chem. C 119 (16) (2015) 8889–8897.

[50] A.P. Bhirud, S.D. Sathaye, R.P. Waichal, L.K. Nikam, B.B. Kale, An eco-friendly, highly stable and efficient nanostructured p-type N-doped ZnO photocatalyst for environmentally benign solar hydrogen production, Green Chem. 14 (10) (2012) 2790–2798.

[51] S. Cao, Y. Chen, C.J. Wang, P. He, W.F. Fu, Highly efficient photocatalytic hydrogen evolution by nickel phosphide nanoparticles from aqueous solution, Chem. Commun. 50 (72) (2014) 10427–10429.

[52] X. Lu, G. Wang, S. Xie, J. Shi, W. Li, Y. Tong, Y. Li, Efficient photocatalytic hydrogen evolution over hydrogenated ZnO nanorod arrays, Chem. Commun. 48 (62) (2012) 7717–7719.

[53] Y. Lv, W. Yao, X. Ma, C. Pan, R. Zong, Y. Zhu, The surface oxygen vacancy induced visible activity and enhanced UV activity of a ZnO 1–x photocatalyst, Catal. Sci. Technol. 3 (12) (2013) 3136–3146.

[54] J. Huo, L. Fang, Y. Lei, G. Zeng, H. Zeng, Facile preparation of yttrium and aluminum co-doped ZnO via a sol–gel route for photocatalytic hydrogen production, J. Mater. Chem. A 2 (29) (2014) 11040–11044.

[55] L. Wei, Y. Chen, Y. Lin, H. Wu, R. Yuan, Z. Li, MoS2 as non-noble-metal co-catalyst for photocatalytic hydrogen evolution over hexagonal ZnIn2S4 under visible light irradiations, Appl. Catal. B 144 (2014) 521–527.
[56] A. Machín, M. Cotto, J. Duconge, J.C. Arango, C. Morant, S. Pinilla, L. Soto-Vázquez, E. Resto, F. Márquez, Hydrogen production via water splitting using different Au@ ZnO catalysts under UV–vis irradiation, J. Photochem. Photobiol. A 353 (2018) 385–394.
[57] S. Choi, J.Y. Do, J.H. Lee, C.S. Ra, S.K. Kim, M. Kang, Optical properties of Cu-incorporated ZnO (CuxZnyO) nanoparticles and their photocatalytic hydrogen production performances, Mater. Chem. Phys. 205 (2018) 206–209.
[58] S. Zhang, X. Yin, Y. Zheng, Enhanced photocatalytic reduction of CO_2 to methanol by ZnO nanoparticles deposited on ZnSe nanosheet, Chem. Phys. Lett. 693 (2018) 170–175.
[59] C. Xin, M. Hu, K. Wang, X. Wang, Significant enhancement of photocatalytic reduction of CO_2 with H_2O over ZnO by the formation of basic zinc carbonate, Langmuir 33 (27) (2017) 6667–6676.
[60] S. Liu, J. Wang, J. Yu, ZIF-8 derived bimodal carbon modified ZnO photocatalysts with enhanced photocatalytic CO_2 reduction performance, RSC Adv. 6 (65) (2016) 59998–60006.